

---

# MULTI-OBJECTIVE LATENT SPACE OPTIMIZATION OF GENERATIVE MOLECULAR DESIGN MODELS

---

**A N M Nafiz Abeer**

Department of Electrical and Computer Engineering  
Texas A&M University  
College Station, TX 77843, USA  
nafiz.abeer@tamu.edu

**Nathan Urban**

Brookhaven National Laboratory  
Computational Science Initiative  
Upton, NY 11973, USA  
nurban@bnl.gov

**M Ryan Weil**

Frederick National Laboratory  
Strategic and Data Science Initiatives  
Frederick, MD 21702, USA  
ryan.weil@nih.gov

**Francis J. Alexander**

Brookhaven National Laboratory  
Computational Science Initiative  
Upton, NY 11973, USA  
falexander@bnl.gov

**Byung-Jun Yoon**

Department of Electrical and Computer Engineering  
Texas A&M University  
College Station, TX 77843, USA  
Brookhaven National Laboratory  
Computational Science Initiative  
Upton, NY 11973, USA  
bjyoon@ece.tamu.edu

March 2, 2022

## ABSTRACT

Molecular design based on generative models, such as variational autoencoders (VAEs), has become increasingly popular in recent years due to its efficiency for exploring high-dimensional molecular space to identify molecules with desired properties. While the efficacy of the initial model strongly depends on the training data, the sampling efficiency of the model for suggesting novel molecules with enhanced properties can be further enhanced via latent space optimization. In this paper, we propose a multi-objective latent space optimization (LSO) method that can significantly enhance the performance of generative molecular design (GMD). The proposed method adopts an iterative weighted retraining approach, where the respective weights of the molecules in the training data are determined by their Pareto efficiency. We demonstrate that our multi-objective GMD LSO method can significantly improve the performance of GMD for jointly optimizing multiple molecular properties.

**Keywords** Generative molecular design (GMD) · variational auto-encoder (VAE) · drug discovery · latent space optimization (LSO) · multi-objective optimization

## 1 Introduction

The development of quantitative structure–activity relationships (QSAR)[1] modeling has accelerated the drug design process. Nevertheless, a typical drug discovery framework like the high-throughput screening (HTS) system[2] still lacks enough computation resources to validate a large number of candidates optimized for multiple properties. Hence, there is always an emphasis on optimizing the candidates for multiple properties, which may be conflicting to each

other, to facilitate the candidate generation process for the HTS system. However, optimization directly over the chemical space is challenging because of the high-dimensionality of the domain, even for a single objective optimization problem. With the advancement of generative networks in modelling the distribution of the input domain, the effective representation in low-dimensional continuous latent space mapped from input space appears to address this challenge. Gómez-Bombarelli et al. [3] use a variational auto-encoder (VAE) to convert the SMILES input sequence into the latent space. Later a Gaussian Process (GP) is modelled on the latent space, and is used in the Bayesian optimization (BO) to come up with optimized molecules. Winter et al. [4] replace the computationally expensive BO with Particle Swarm Optimization (PSO) and tries to optimize multiple properties in a weighted-combination manner. Often, the input data is distributed over a wide range of properties. Hence, the latent space may not fully represent the chemical space with the desired properties and the optimization procedure goes towards invalid regions away from the learned space. To deal with this lack of knowledge in the latent space, constraints[5, 6] related to the validity of the samples are imposed on the optimization. Kang et al. [7] propose the decoder of a semi-supervised variational autoencoder to be conditioned by the property values and is able to construct the latent space centered around a desired range of multiple properties.

Another prevailing approach involves training a generative network to model the input data distribution followed by a fine tuning via reinforcement learning (RL) to meet the design criteria. Olivecrona et al.'s [8] fine tuning facilitates the generation of high scoring molecules without deviating away from the actual input distribution. Shi et al. [9] apply RL policy to fine tune the molecular graph generating network. In the objective-reinforced generative adversarial network (ORGAN) [10] framework, the reward for generating molecules with better property is assimilated into the loss function to guide the latent space distribution during training. To remove any possible bias in the generative network from a training dataset, Zhou and his colleagues[11] frame the molecular generation as a Markov Decision Process (MDP) and utilize the objective value as the reward for the Deep Q-network [12] to find a policy for the MDP. The domain knowledge from chemistry dictates the possible actions for the MDP to ensure the validity of the generated molecule. For multi-objective optimization, they also employ the weighted combination of multiple objectives according to the design expectation.

To improve the quality of the molecules from the latent space, Yang et al. [13] propose an iterative retraining approach where they pre-train the generative model jointly with a property predictor. Later this predictor selects a small number of top molecules and they are added to the initial dataset so that the latent space is adjusted to these candidate molecules. Liu et al. [14] iteratively update the generator in GAN under a chance-constrained optimization framework. They employ a validity function to guide the optimization of the property value within region of grammatically correct input sequences or structures. Tripp et al. [15] introduces the concept of weighted retraining a pre-trained model to reshape its latent space where the weights of the training samples are controlled by the rank of the objective values. Their framework can address the multi-objective optimization for a combined objective score (i.e. penalized logP). A recent iterative approach [16] in material design applies genetic algorithm (GA) along with some domain knowledge to generate the possible optimized micro-structures from the initial training data. The property values of these candidates are validated by the high-throughput experiments or simulations. A deep neural network (DNN) property predictor is then retrained with a larger dataset augmented by the candidates from GA. In contrast to the generative approach, the candidates from GA remain closer to the training data. Hence, the predictions from DNN are quite reliable. However, the use of experiments to reevaluate the property of the candidates is still a challenge to be addressed for a large dataset.

In the previous works mentioned so far, the multi-objective optimization is usually converted into a single objective optimization with the use of a preference weight vectors. However, the selection of the weights guides the optimization along a preferred direction usually set by the designer. This often leads to the candidates which are optimized dominantly by one of the objectives. It is worth noting that Gopakumar et al. [17] use a measure of expected improvement in terms of the Pareto Fronts in the objective space for an efficient experiment design. We have extended the weighted retraining framework of Tripp et al. [15] to address the multi-objective optimization. Our approach (Figure 1) considers the set of all Pareto optimal candidate solutions to the optimization problem and effectively advances the latent space towards a wider region in the objective space. Our primary contribution is incorporating the notion of Pareto Fronts in the objective space to form the weighted dataset. Secondly, our experimental results for different property pairs signify the capability of the weighted retraining in the multi-objective optimization. Specially, the approach seems to overcome the challenges of a dataset with inadequate sample-representation of the domain space.

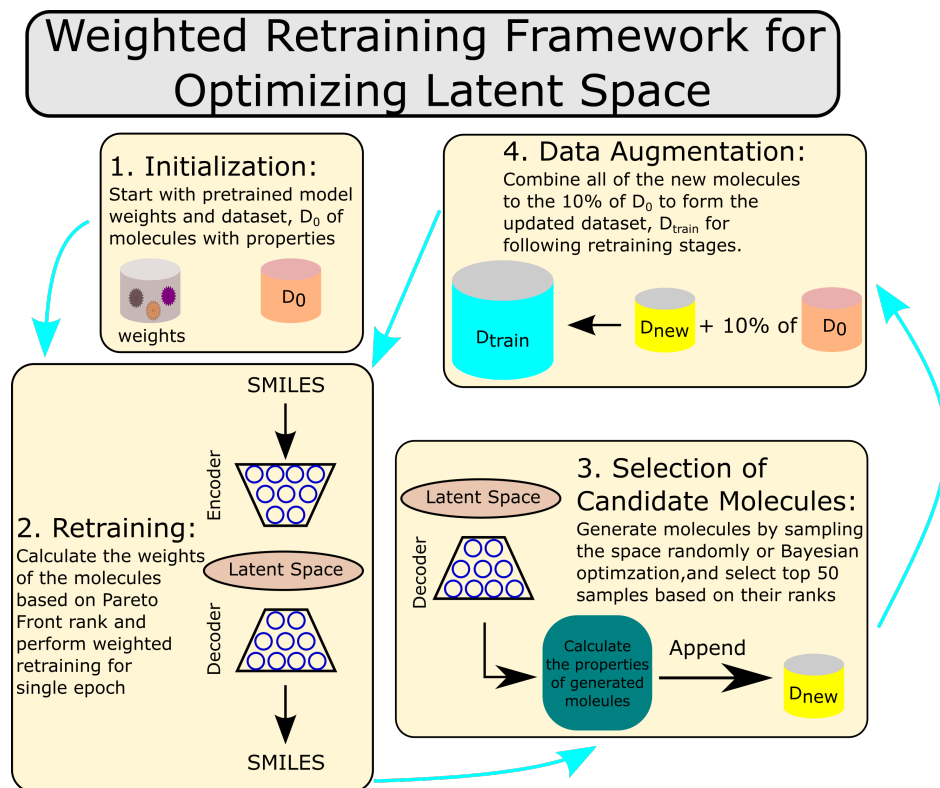


Figure 1: **Multi-objective latent space optimization through retraining based on Pareto front rank.** Initialization involves using a JT-VAE model trained with the initial dataset. Then stage 2,3,4 are repeated sequentially for a fixed number of iterations. In stage 3, the model retrained with weighted dataset at stage 1 is explored randomly or via Bayesian Optimization to select the candidates. These new molecules are added to training dataset in Data Augmentation for next retraining.

## 2 Methods

### 2.1 Overview of the Proposed Method

Given an initial dataset of molecules with properties of interests and a baseline generative model trained with that dataset, we make use of the Pareto Front concept to create a ranking among the training samples. Section 2.2 provides a detailed description of the algorithm to rank these molecules based on their objective values. To fine-tune the baseline model’s latent space towards the high ranking molecules, we form a weighted-dataset by turning the ranks into weights in a fashion such that high ranking samples gets larger weights. The baseline model is then retrained with this weighted-dataset for a single epoch and becomes the exploration field for proposing new molecules with optimum properties, preferable better than those in the initial dataset. We choose a small number (50) of points from the latent space randomly or using the multi-objective Bayesian Optimization technique. At this stage, we use predictive models to calculate the properties of the proposed molecules, decoded from the selected latent points and create a candidate dataset with these molecules.

Before initiating the retraining again, we incorporate the candidates into the training data by combining with 10% of the initial dataset. Subsequently, the generative network gets retrained with the weighted dataset and a new set of molecules are proposed to be appended to the candidate dataset. This periodic weighted retraining, followed by candidate generation and data augmentation can be repeated until either our proposed molecules meet the expectation in the objective space or we reach the convergence in the properties of the designed molecules. We have described this iterative retraining procedure in details in Section 2.3.

## 2.2 Pareto Front Rank

In the multi-objective optimization framework, not all solutions have better performance in every objective. The reason behind that is achieving a good score in certain objective function does not always guarantee similar trend in the other objectives. Hence, instead of getting a single solutions, we have to work with Pareto Optimal set defined as the collection of solutions which are not dominated by any other points in feasible objective space.[18] A point  $x^i$  dominates another point  $x^j$  if 1)  $x^i$  cannot underperform than  $x^j$  in all objectives, and 2)  $x^j$  is strictly worse than  $x^i$  in at least one performance criterion. All of the points in the Pareto Optimal set in the design space form the Pareto Front in the objective space. Considering all performance criteria, these points in the Pareto Front are the optimum solutions and they hold the same rank among all possible solutions.

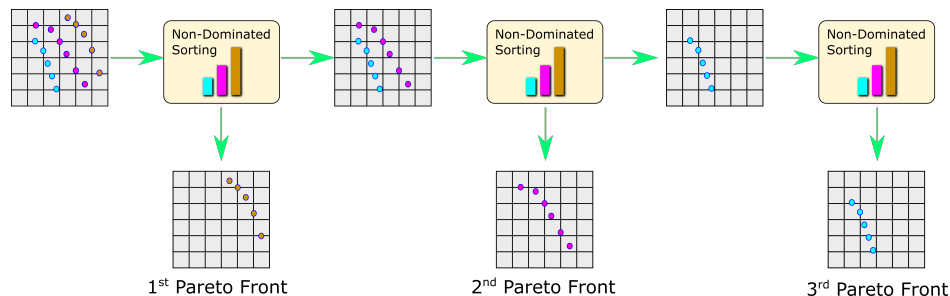


Figure 2: **Illustration of Pareto Front Rank Estimation:** The datapoints are showed in the objective space where our expectation is the larger values for both objectives. The Non-Dominated Sorting is applied sequentially until all Pareto Fronts (which is 3 in the Figure) are extracted.

For a given set of datapoints (molecules in our work) with their scores in certain objectives, we can find out all possible Pareto Optimal sets,  $P_1, P_2, P_3, \dots$  using the **Algorithm 2** (Figure 2). Here, the **Algorithm 1** is iteratively used on updated set of points to find the non-dominated set or the Pareto Optimal points until the set of points is exhausted. Once we have extracted all the Pareto Fronts, we can determine the Pareto Front rank of the datapoints according to the equation 1.

$$rank(x) = \sum_{i=1}^{j-1} |P_i| \quad \forall x \in P_j \quad (1)$$

---

### Algorithm 1 Algorithm for Identifying Non-dominated Set of Points

---

**Require:** N datapoints with their objective scores

Initialize  $P' = \{1, 2, 3, \dots, N\}$

▷ Set of Non Dominated points,  $P'$

and  $i \leftarrow 1$

**while**  $i \leq |P'|$  **do**

Initialize  $k \leftarrow 0$

**for** (each  $j \in P' \wedge j \neq i$ ) **do**

**if** ( $x^{(j)}$  does not dominate  $x^{(P'(i))}$  in any objective score) **then**

$P' \leftarrow P' \setminus \{j\}$

**else if**  $j < i$  **then**

$k \leftarrow k + 1$

**end if**

$i \leftarrow k + 1$

**end for**

**end while**

---

## 2.3 Deep Generative Model for Molecular Design: JT-VAE

We have used the Junction Tree Variational Autoencoder (JT-VAE) architecture due to its effective molecule generation process from the latent space. JT-VAE encodes the SMILES into a latent space formed by the graph and the tree structure. At the graph generation step, the decoded tree structure works as an anchor to guide the decoding of the

**Algorithm 2** Algorithm for Non-dominating Sorting of Datapoints**Require:** N datapoints with their objective scoresInitialize  $P = \{1, 2, 3, \dots, N\}$ ,  $j = 1$ **while**  $|P| \neq 0$  **do**    **Step 1:** Find the non-dominated set,  $P'$  from  $P$  using **Algorithm 1**.    **Step 2:**  $P_j \leftarrow P'$ ,  $P \leftarrow P \setminus P'$  and  $j \leftarrow j + 1$  $\triangleright P_j : j^{th}$  Pareto Front**end while**

latent space corresponding to the graph structure. This results in producing a higher fraction of valid molecules with the maximum reconstruction accuracy compared to the other VAE models. [19]

We have moderated the weighted retraining implemented in Tripp et al. [15] by augmenting the dataset in a manner such that all the new molecules generated by the model contribute in the retraining irrespective of their rankings. We start with initial dataset,  $\mathcal{D}_0$  and a null set,  $\mathcal{D}_{new}$  of the new molecules suggested by the model. After the first weighted retraining with  $\mathcal{D}_{train} = \mathcal{D}_0$ , we randomly generate 250 molecules from the latent space of the model and append the top 20% of them to  $\mathcal{D}_{new}$ . For rest of the retraining stages, we have used a dataset,  $\mathcal{D}_{train} = \mathcal{D}'_0 \cup \mathcal{D}_{new}$ , where  $\mathcal{D}'_0$  is the 10% molecules randomly sampled from the  $\mathcal{D}_0$  according to the ranks and  $\mathcal{D}_{new}$  is the updated set of new molecules. We have used the rank information (equation 1) to form the weights for each sample,

$$w(x, k, \mathcal{D}) = \frac{1}{kN + rank_{\mathcal{D}}(x)} \quad (2)$$

The parameter  $k$  controls the flow of rank information into the sample weights. Reducing from a very large value of  $k$  to closer to zero transforms the uniform weight distribution to be centered around the high-ranking datapoints.

The pre-trained JT-VAE, shared by Tripp et al. [15] is the baseline model for the Task 1. In the second task, we needed to train the JT-VAE models for each partial dataset formed by eliminating the top 20% molecules from the complete dataset that we have used in the previous task. For all of these models, a learning rate of 0.0007 is used with batch size of 32 for 30 epochs.

## 2.4 DRD2 Activity Classifier

The surrogate model for predicting the activity against the dopamine type 2 receptor DRD2, is built as a binary Support Vector Machine (SVM) classifier with a radial basis function ( $\gamma = 2^{-6}$ ). The Morgan Fingerprint, with radius 3 (FCFC6) computed by RDKit[20] are used as the input features for the SVM classifier. The probability of being active predicted by this model for each molecules is treated as a property to be maximized.

Dataset	Accuracy	ROC-AUC
Train	0.9998	0.9999
Validation	0.9807	0.8745
Test	0.9842	0.9074

Table 1: Performance of the trained SVM model

Since there is a class imbalance issue due to the smaller number of active molecules, Olivecrona et al. [8] split the active samples in such a way that the structural similarity among the samples from the train and test/validation dataset is less. We have used the same split dataset consisting of 7218 actives and 100000 inactive molecules to train, test and validate the SVM model in Scikit-learn, 0.23.2[21] with a regularization parameter,  $C = 2^7$ . The mean accuracy of the classifier used in this work is mentioned in Table 1 for the train, validation and test set.

## 2.5 Data

The specific training and validation split of the ZINC dataset provided in <https://github.com/cambridge-mlg/weighted-retraining> is used in this work for retraining JT-VAE.

### 3 Results and Discussion

We have chosen water-octanol partition coefficient (logP), synthetic accessibility score (SAS), natural product-likeness score (NP score)[22] and the probability of activity against DRD2 as the drug properties to be optimized. All properties except SAS are targeted for maximization. In our work, logP and the SAS values for all molecules are calculated with RDKit package[20] whereas we have used surrogate models for other two properties. Particularly, the method for determining natural product-likeness score described in [22] is followed to compute NP score from the SMILES. Details of predictive model for probability against DRD2 activity is given in "Methods" section.

We have categorized the experiments into three tasks. For the first two tasks, the random selection of latent space molecules produces the candidates for next retraining stage. To analyze the effect of the dataset, we have used a smaller dataset in the second task by omitting top 20% molecules according to their Pareto Front rank. In the final task, a Bayesian optimization replaces the random selection in Task 1.

#### 3.1 Weighted retraining via Pareto front rank effectively shifts the latent space for multiple objectives

We have started weighted training the baseline model with the complete ZINC dataset[23] where the train-validation split is same as in the work of Tripp et al.[15]. After each retraining step,  $r = 50$  candidates are selected from 250 randomly generated molecules based on the Pareto Front rank and they participate in the following retraining stages. For details, please see the "Methods" section.

Figure 3 illustrates the effect of the weight parameter  $k$  on the latent space optimization for logP, SAS pair. We retrain the baseline model 10 times using the Pareto Front rank with different values of  $k$ , and collect 1000 molecules randomly from the latent space to plot the distribution of the properties of the latent space molecules. Additionally, the initial training data and 1000 random samples from the latent space of the baseline model are included to show the relative improvement of the weighted retraining. As the retraining progresses, the logP distribution of the latent space shifts towards the positive values whereas the SAS values becomes more concentrated below 2. Also, for lower values of  $k$ , the change in the distribution becomes more significant. The cases for very smaller  $k$  (i.e.  $10^{-5}$ ,  $10^{-6}$ ) produce the multi-modal property distributions. Here, the model learns the latent space for a few Pareto Fronts as the weights become more dependent on the ranks for  $k$  closer to 0. Consequently, the latent space becomes clustered around high ranking molecules which are located on wider Pareto Fronts.

The average property values for the training data, 1000 molecules generated from the initial model and retrained model for different values of weight parameter  $k$  are reported in the Table 2 in **Appendix**. We have also calculated the structural diversity of the generated molecules from different version of JT-VAE models to verify that the model is able to learn wider chemical space. The diversity is defined as the average structural distance (ECFC4) between nearest molecules in set of molecules. For values of  $k$  closer to zero, we observe that the structural diversity is reduced. Since smaller  $k$  enables the weights of the samples to be more influenced by their ranks, the model sees the high-ranking molecules more frequently. Consequently, it mostly learns the particular region in latent space corresponding to optimum molecules and the diversity of the latent space decreases.

#### 3.2 Multi-objective latent space optimization effectively recovers sampling efficiency for incomplete dataset

In this task, we seek to analyze the performance of the weighted retraining approach when the training data lacks better samples. At first, we remove the top 20% molecules from the training data used to train the baseline model[15]. Since the baseline model from Task 1, has seen the complete dataset during its training, we train separate baseline models with the reduced dataset for each property pairs.

The scatter plots in Figure 4 compare the progression of the properties in Task 1 and Task 2 for logP and SAS pair with  $k = 10^{-5}$ . Although the initial data of the second task does not contain many molecules with logP greater than 4 and SAS lower than 2 as in Task 1, the weighted training still manages to push the latent space towards same region as it does for the complete dataset.

#### 3.3 Discovery of DRD2 active molecules using optimized generative models

To see the performance of the proposed approach in extreme situation, we consider the DRD2 property along with a property from logP, SAS and NP score. When we exclude the top 20% molecules based on the Pareto Front rank, we eventually end up with an initial dataset which provides no knowledge about the active DRD2 molecules. Moreover, the baseline model has not seen those active molecules either. Hence, this optimization task essentially is asking the weighted-retraining to guide the latent space towards a completely unexplored region.

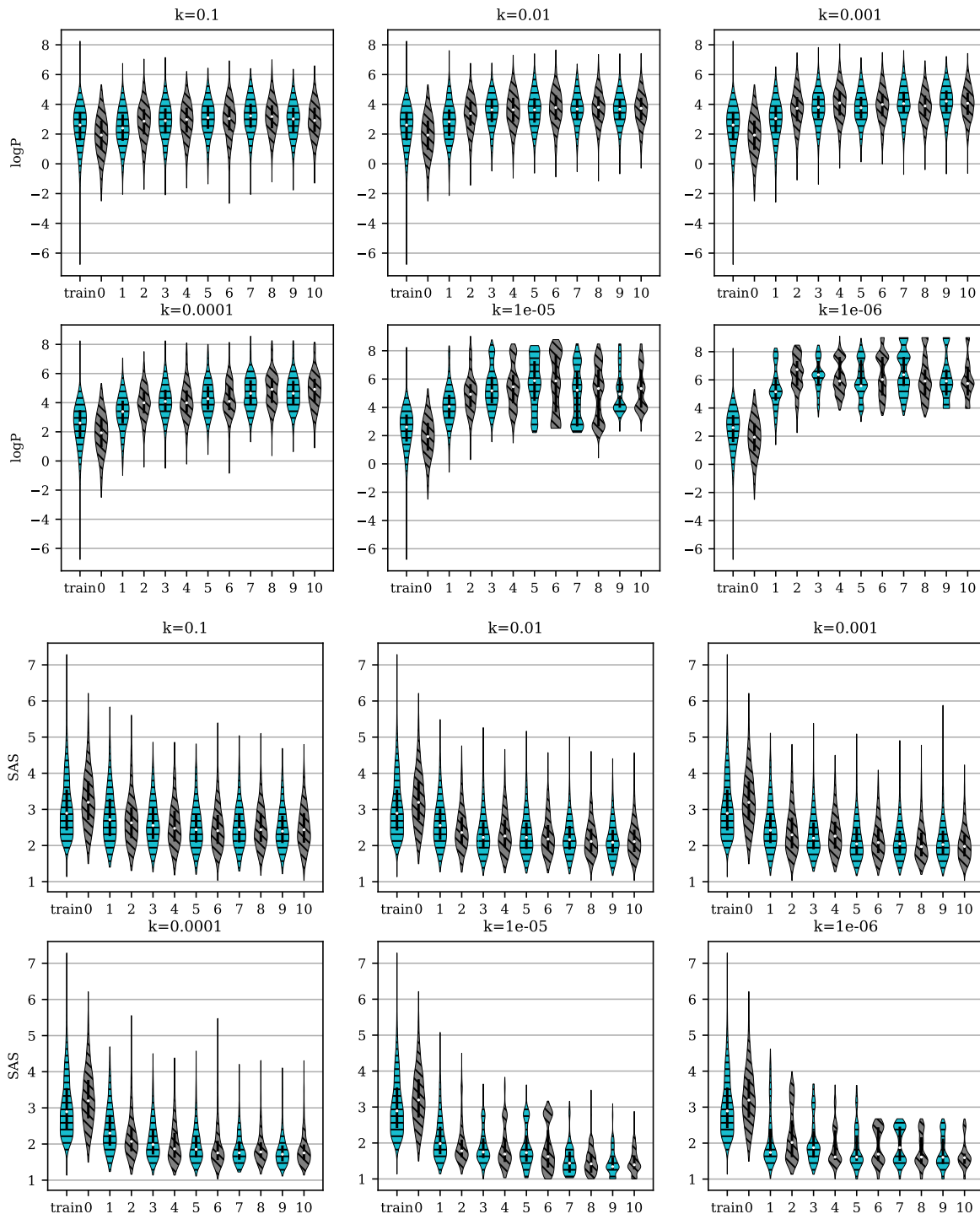


Figure 3: **Progression of Property Distribution for logP and SAS in Task 1:** The logP and SAS distribution of the training data and the randomly sampled 1000 molecules from the baseline model and the retrained model after each weighted retraining for all six values of  $k$ . The ‘train’ and ‘0’ labels indicate the training data and the sampled molecules from the baseline model respectively. The other labels, ‘1-10’ are for the models after each retraining stage.

We apply the weighted-retraining with the goal of maximizing the probability of activity against the DRD2 and optimizing another property simultaneously. For proposing candidates from the latent space, we first randomly select

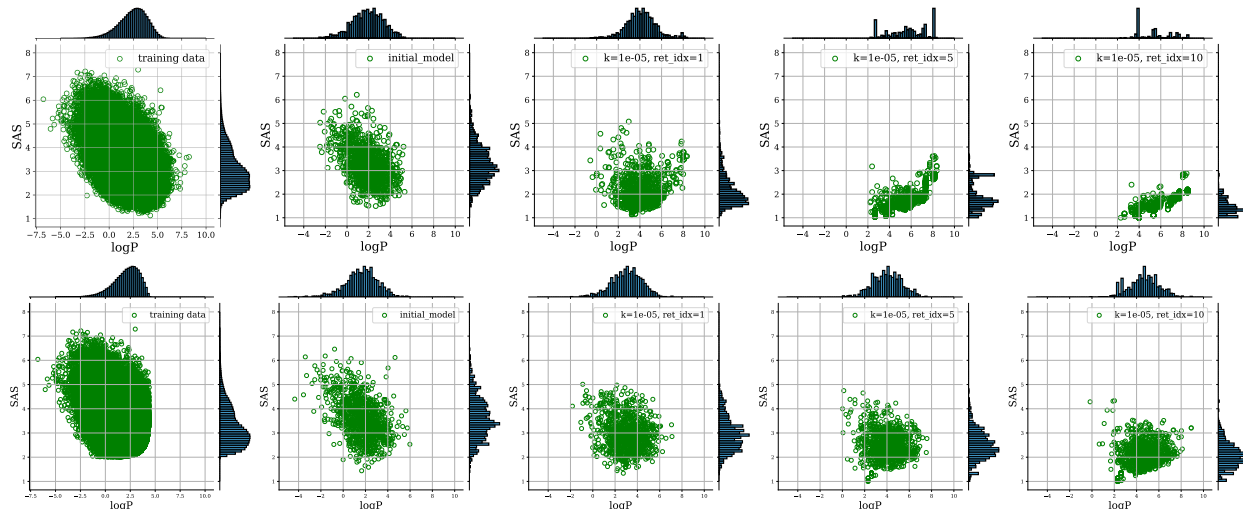


Figure 4: **Transition of logP and SAS towards optimum direction in Task 1 and 2:** The first two scatter plots in each row represent the training data and the molecules generated from the baseline model respectively. In rest of the jointplots, the molecules from learned model after 1<sup>st</sup>, 5<sup>th</sup> and 10<sup>th</sup> weighted retraining for  $k = 10^{-5}$  are shown in the objective space. The top and bottom rows are showing the trend for starting with complete dataset (Task 1) and reduced dataset (Task 2) respectively.

250 latent points and decode them back to the chemical space. Afterwards, we employ the surrogate models to predict the DRD2 activity probability and logP, SAS or NP score for these random molecules. Based on the Pareto Front ranks, top 50 candidates are selected for the succeeding retraining stages. Out of these 50 samples, we discard those samples that are either with invalid chemical structure or already in the training dataset. Thus, the candidate dataset becomes a collection of novel molecules with possibly better properties. The results for the weighted retraining with  $k = 10^{-6}$

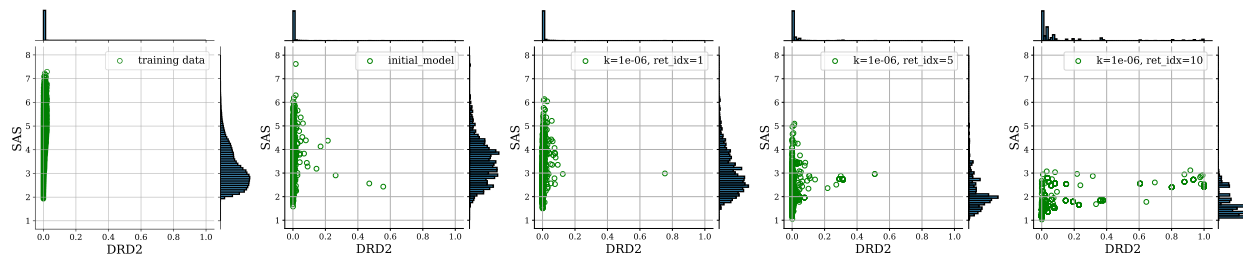
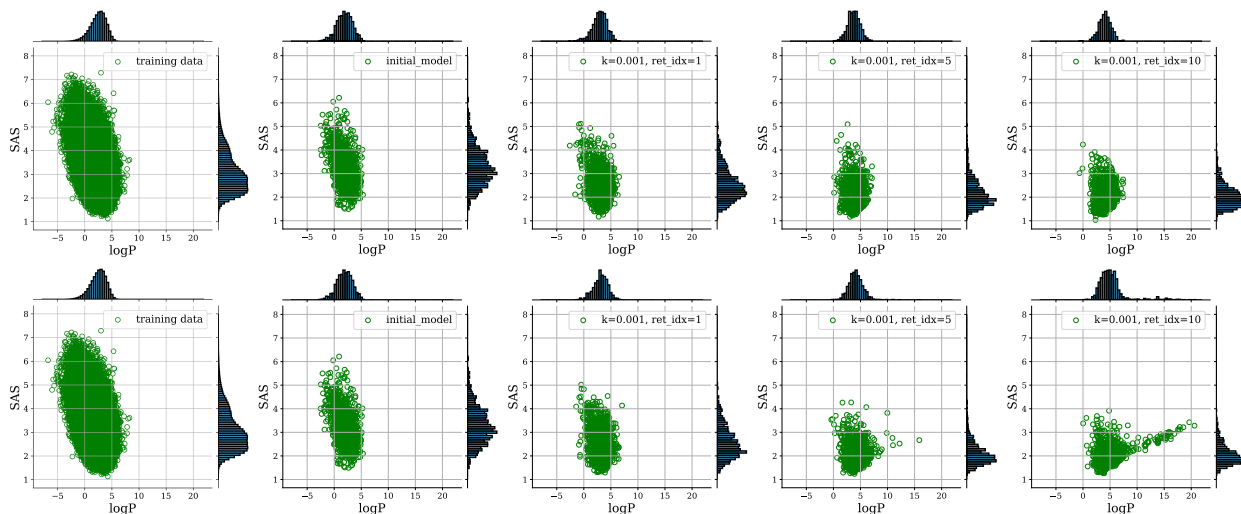


Figure 5: **Transition of DRD2 and SAS towards optimum direction in Task 2:** The first two scatter plots represent the training data and the molecules generated from the baseline model respectively. In rest of the jointplots, the molecules from learned model after 1<sup>st</sup>, 5<sup>th</sup> and 10<sup>th</sup> weighted retraining for  $k = 10^{-6}$  are shown in the objective space.

is shown in Figure 5 for DRD2 and SAS pair. Here, the properties of 1000 molecules randomly generated from the trained latent space after 10<sup>th</sup> retraining stage demonstrate that the latent space is able to produce a small number of molecules with higher probability of being active against DRD2. Additionally, the SAS distribution of the sampled molecules becomes more skewed towards smaller values as expected. However, the active molecules have slightly higher SAS than the average of the latent space. We have repeated this task for other pairs associated with logP and NP score. The weighted retraining scheme also succeeds in producing active molecules for those pairs. (Table 3 of Appendix for details)

### 3.4 Molecule optimization and selection via Bayesian optimization can enhance latent space optimization results

In previous tasks, the training data gets augmented by molecules which have higher ranks among the randomly selected samples. To improve the quality of the new candidate molecules, the Bayesian optimization on the latent space may



**Figure 6: Effect of Bayesian optimization on the progression of the model in the objective space:** The first and second rows represent the scatter plots for random selection and Bayesian optimization strategy respectively. In each row, the objective space are for the training data, the molecules from the baseline model and retrained model after 1<sup>st</sup>, 5<sup>th</sup> and 10<sup>th</sup> weighted retraining for  $k = 10^{-3}$ .

provide better candidates than the random selection. To validate this claim, we apply the Bayesian optimization on the latent space with the logP value penalized by the SAS as the objective function. The logP and SAS values are standardized using the mean and the standard deviation of the initial dataset. Figure 6 illustrates that for  $k = 10^{-3}$ , the random selection can not go very far from the baseline model. At the expense of computational complexity, the Bayesian optimization shifts the latent space to the higher logP regions. Since the objective function is a linear combination of logP and SAS, the candidate molecules suggested by the optimization gets biased towards the higher logP region with higher SAS. A well designed objective function or use of multi-objective Bayesian optimization may resolve this issue. Nonetheless, this weighted-objective formulation indeed shows the advantage of the Bayesian optimization in searching for the candidate molecules.

## 4 Conclusion

The presented framework for multi-objective optimization illustrates the potential of weighted retraining in bringing the molecule generation model in the expected multi-dimensional objective region. The JT-VAE model’s latent space is optimized for different pairs of molecular properties and the effect of ranks are studied. We have found that the weight formulation from the ranks dictates a trade-off between the diversity and the shifts of the property distribution in the latent space. To verify the strength of our approach, similar experiments are repeated with having relatively poor training data. Even starting with no DRD2 active molecules, weighted retrained models still manage to configure its latent space for the active region. These outcomes are more pronounced given the fact that random selection from the latent space is used to propose the candidate molecules for retraining stages. To speed up the reshaping of the latent space, the Bayesian optimization is showed to be promising.

The ranking scheme of our framework is contingent on the robust property predictors. How well these surrogate models can tackle the unexplored chemical space is critical. Even if these models are less accurate, the retrained latent space can still be the exploration field for further screening. Given a reliable and fast approximate mapping from molecule to its property value, the weighted retraining approach can optimize the latent space jointly for more practical properties that are responsible for higher attrition rate of proposed drugs. With the availability of the surrogate models for protein-ligand binding score [24], inhibition of bile salt export pump [25], our approach can optimize the latent space in producing candidate drugs that are most likely to be active against specific target without causing possible damage to the patients. In terms of computational cost, retraining the generative network multiple times may be slightly expensive for larger network compared to the one we have used. However, with the application of distributed training [26], the training time can be significantly mitigated. Moreover, we have seen a decreasing trend in diversity of the molecules of the latent space with the increase in the property distribution. A diversity-oriented candidate selection strategy could be a better answer to this issue.

As shown in Fig. 6, the latent space optimization outcomes can be enhanced by adopting more effective sampling strategies in the latent space that can identify and suggest novel molecules with more desirable properties. In this study, this was demonstrated by replacing the random sampling scheme with Bayesian optimization. In fact, it may be possible to further improve the GMD through the proposed multi-objective LSO scheme by incorporating more sophisticated optimization techniques that can effectively explore the unknown landscape of the multiple objective functions under immense uncertainties. Optimal experimental design (OED) [27, 28, 29, 30] and active learning [31, 32, 33] techniques that build on objective-based uncertainty quantification (objective-UQ) based on MOCU (mean objective cost of uncertainty) [34, 35] may provide practical solutions for such “uncertainty-aware” sampling in the latent space. These are topics of our ongoing investigation.

## Author Contributions

FJA, BJY, NU initiated the project. BJY, NU proposed the idea. NA developed, refined, evaluated the method. MRW evaluated the efficacy of the predicted molecules. NA, BJY analyzed the results and wrote the paper. All authors have edited and verified the paper.

## References

- [1] Eugene N. Muratov, Jürgen Bajorath, Robert P. Sheridan, Igor V. Tetko, Dmitry Filimonov, Vladimir Poroikov, Tudor I. Oprea, Igor I. Baskin, Alexandre Varnek, Adrian Roitberg, Olexandr Isayev, Stefano Curtalolo, Denis Fourches, Yoram Cohen, Alan Aspuru-Guzik, David A. Winkler, Dimitris Agrafiotis, Artem Cherkasov, and Alexander Tropsha. Qsar without borders. *Chem. Soc. Rev.*, 49:3525–3564, 2020.
- [2] Edward H. Kerns. High throughput physicochemical profiling for drug discovery. *Journal of Pharmaceutical Sciences*, 90(11):1838–1858, 2001.
- [3] Rafael Gómez-Bombarelli, Jennifer N Wei, David Duvenaud, José Miguel Hernández-Lobato, Benjamín Sánchez-Lengeling, Dennis Sheberla, Jorge Aguilera-Iparraguirre, Timothy D Hirzel, Ryan P Adams, and Alán Aspuru-Guzik. Automatic chemical design using a data-driven continuous representation of molecules. *ACS central science*, 4(2):268—276, February 2018.
- [4] Robin Winter, Floriane Montanari, Andreas Steffen, Hans Briem, Frank Noé, and Djork-Arné Clevert. Efficient multi-objective molecular optimization in a continuous latent space. *Chem. Sci.*, 10:8016–8024, 2019.
- [5] Ryan-Rhys Griffiths and José Miguel Hernández-Lobato. Constrained bayesian optimization for automatic chemical design using variational autoencoders. *Chem. Sci.*, 11:577–586, 2020.
- [6] Pascal Notin, José Miguel Hernández-Lobato, and Yarin Gal. Improving black-box optimization in vae latent space using decoder uncertainty, 2021.
- [7] Seokho Kang and Kyunghyun Cho. Conditional molecular design with deep generative models. *Journal of Chemical Information and Modeling*, 59(1):43–52, Jan 2019.
- [8] Marcus Olivecrona, Thomas Blaschke, Ola Engkvist, and Hongming Chen. Molecular de-novo design through deep reinforcement learning. *Journal of Cheminformatics*, 9(1), 2017.
- [9] Chence Shi, Minkai Xu, Zhaocheng Zhu, Weinan Zhang, Ming Zhang, and Jian Tang. Graphaf: a flow-based autoregressive model for molecular graph generation, 2020.
- [10] Benjamin Sanchez-Lengeling, Carlos Outeiral, Gabriel Guimaraes, and Alan Aspuru-Guzik. Optimizing distributions over molecular space. an objective-reinforced generative adversarial network for inverse-design chemistry (organic), 2017.
- [11] Zhenpeng Zhou, Steven Kearnes, Li Li, Richard N. Zare, and Patrick Riley. Optimization of molecules via deep reinforcement learning. *Scientific Reports*, 9(1):10752, Jul 2019.
- [12] Volodymyr Mnih, Koray Kavukcuoglu, David Silver, Andrei A. Rusu, Joel Veness, Marc G. Bellemare, Alex Graves, Martin Riedmiller, Andreas K. Fidjeland, Georg Ostrovski, Stig Petersen, Charles Beattie, Amir Sadik, Ioannis Antonoglou, Helen King, Dharshan Kumaran, Daan Wierstra, Shane Legg, and Demis Hassabis. Human-level control through deep reinforcement learning. *Nature*, 518(7540):529–533, Feb 2015.
- [13] Kevin Yang, Wengong Jin, Kyle Swanson, Dr.Regina Barzilay, and Tommi Jaakkola. Stochastic iterative target augmentation. In Hal Daumé III and Aarti Singh, editors, *Proceedings of the 37th International Conference on Machine Learning*, volume 119 of *Proceedings of Machine Learning Research*, pages 10716–10726. PMLR, 13–18 Jul 2020.

- [14] Xianggen Liu, Qiang Liu, Sen Song, and Jian Peng. A chance-constrained generative framework for sequence optimization. In Hal Daumé III and Aarti Singh, editors, *Proceedings of the 37th International Conference on Machine Learning*, volume 119 of *Proceedings of Machine Learning Research*, pages 6271–6281. PMLR, 13–18 Jul 2020.
- [15] Austin Tripp, Erik Daxberger, and José Miguel Hernández-Lobato. Sample-efficient optimization in the latent space of deep generative models via weighted retraining, 2020.
- [16] Yongtae Kim, Youngsoo Kim, Charles Yang, Kundo Park, Grace X. Gu, and Seunghwa Ryu. Deep learning framework for material design space exploration using active transfer learning and data augmentation. *npj Computational Materials*, 7(1):140, Sep 2021.
- [17] Abhijith M. Gopakumar, Prasanna V. Balachandran, Dezhen Xue, James E. Gubernatis, and Turab Lookman. Multi-objective optimization for materials discovery via adaptive design. *Scientific Reports*, 8(1):3738, Feb 2018.
- [18] Kalyanmoy Deb. *Multi-objective optimization using evolutionary algorithms*. John Wiley & Sons, 2004.
- [19] Wengong Jin, Regina Barzilay, and Tommi S. Jaakkola. Junction tree variational autoencoder for molecular graph generation. In Jennifer G. Dy and Andreas Krause, editors, *Proceedings of the 35th International Conference on Machine Learning, ICML 2018, Stockholmsmässan, Stockholm, Sweden, July 10-15, 2018*, volume 80 of *Proceedings of Machine Learning Research*, pages 2328–2337. PMLR, 2018.
- [20] Greg Landrum. Open-source cheminformatics software.
- [21] F. Pedregosa, G. Varoquaux, A. Gramfort, V. Michel, B. Thirion, O. Grisel, M. Blondel, P. Prettenhofer, R. Weiss, V. Dubourg, J. Vanderplas, A. Passos, D. Cournapeau, M. Brucher, M. Perrot, and E. Duchesnay. Scikit-learn: Machine learning in Python. *Journal of Machine Learning Research*, 12:2825–2830, 2011.
- [22] Peter Ertl, Silvio Roggo, and Ansgar Schuffenhauer. Natural product-likeness score and its application for prioritization of compound libraries. *Journal of Chemical Information and Modeling*, 48(1):68–74, 2007.
- [23] John J. Irwin, Teague Sterling, Michael M. Mysinger, Erin S. Bolstad, and Ryan G. Coleman. Zinc: A free tool to discover chemistry for biology. *Journal of Chemical Information and Modeling*, 52(7):1757–1768, 2012.
- [24] Derek Jones, Hyojin Kim, Xiaohua Zhang, Adam Zemla, Garrett Stevenson, W. F. Drew Bennett, Daniel Kirshner, Sergio E. Wong, Felice C. Lightstone, and Jonathan E. Allen. Improved protein–ligand binding affinity prediction with structure-based deep fusion inference. *Journal of Chemical Information and Modeling*, 61(4):1583–1592, 2021. PMID: 33754707.
- [25] Kevin S. McLoughlin, Claire G. Jeong, Thomas D. Sweitzer, Amanda J. Minnich, Margaret J. Tse, Brian J. Bennion, Jonathan E. Allen, Stacie Calad-Thomson, Thomas S. Rush, and James M. Brase. Machine learning models to predict inhibition of the bile salt export pump. *Journal of Chemical Information and Modeling*, 61(2):587–602, 2021. PMID: 33502191.
- [26] Sam Ade Jacobs, Tim Moon, Kevin McLoughlin, Derek Jones, David Hysom, Dong H Ahn, John Gyllenhaal, Pythagoras Watson, Felice C Lightstone, Jonathan E Allen, Ian Karlin, and Brian Van Essen. Enabling rapid covid-19 small molecule drug design through scalable deep learning of generative models. *The International Journal of High Performance Computing Applications*, 35(5):469–482, 2021.
- [27] Roozbeh Dehghannasiri, Byung-Jun Yoon, and Edward R Dougherty. Optimal experimental design for gene regulatory networks in the presence of uncertainty. *IEEE/ACM Transactions on Computational Biology and Bioinformatics*, 12(4):938–950, 2014.
- [28] Roozbeh Dehghannasiri, Byung-Jun Yoon, and Edward R Dougherty. Efficient experimental design for uncertainty reduction in gene regulatory networks. In *BMC Bioinformatics*, volume 16, pages 1–18. Springer, 2015.
- [29] Youngjoon Hong, Bongsuk Kwon, and Byung-Jun Yoon. Optimal experimental design for uncertain systems based on coupled differential equations. *IEEE Access*, 9:53804–53810, 2021.
- [30] Hyun-Myung Woo, Youngjoon Hong, Bongsuk Kwon, and Byung-Jun Yoon. Accelerating optimal experimental design for robust synchronization of uncertain kuramoto oscillator model using machine learning. *IEEE Transactions on Signal Processing*, 69:6473–6487, 2021.
- [31] Guang Zhao, Edward Dougherty, Byung-Jun Yoon, Francis J Alexander, and Xiaoning Qian. Efficient active learning for gaussian process classification by error reduction. In *Thirty-fifth Conference on Neural Information Processing Systems*, 2021.
- [32] Guang Zhao, Edward Dougherty, Byung-Jun Yoon, Francis Alexander, and Xiaoning Qian. Uncertainty-aware active learning for optimal bayesian classifier. In *International Conference on Learning Representations*, 2021.

- [33] Guang Zhao, Edward Dougherty, Byung-Jun Yoon, Francis J Alexander, and Xiaoning Qian. Bayesian active learning by soft mean objective cost of uncertainty. In *International Conference on Artificial Intelligence and Statistics*, pages 3970–3978. PMLR, 2021.
- [34] Byung-Jun Yoon, Xiaoning Qian, and Edward R Dougherty. Quantifying the objective cost of uncertainty in complex dynamical systems. *IEEE Transactions on Signal Processing*, 61(9):2256–2266, 2013.
- [35] Byung-Jun Yoon, Xiaoning Qian, and Edward R Dougherty. Quantifying the multi-objective cost of uncertainty. *IEEE Access*, 9:80351–80359, 2021.

## A Performance of weighted retraining for six pairs of properties

### A.1 Effect of weight parameter $k$ in Task 1

Pair	Property	Training data	Initial Model	Model after $10^{th}$ retraining with					
				$k = 10^{-1}$	$k = 10^{-2}$	$k = 10^{-3}$	$k = 10^{-4}$	$k = 10^{-5}$	$k = 10^{-6}$
logP, SAS	logP	2.4583	1.892	2.9349	3.6783	4.0592	4.8422	5.2963	6.0017
	logP (top 10%)	4.6321	4.2461	4.9848	5.6109	5.9546	7.018	8.0196	8.9998
	SAS	3.0535	3.2642	2.5012	2.1818	2.047	1.8387	1.4716	1.6566
	SAS (top 10%)	1.9545	2.0544	1.5789	1.4669	1.4112	1.3475	1.004	1.1522
	Structural Diversity		0.8356	0.7904	0.7512	0.7309	0.6773	0.6205	0.6126
logP, NP score	logP	2.4583	1.892	2.8972	3.2708	3.6407	4.0105	6.0847	6.3781
	logP (top 10%)	4.6321	4.2461	5.0467	5.5148	5.992	6.4334	8.1291	7.9213
	NP_score	-1.3122	-1.0196	-0.7303	-0.4854	-0.2257	0.3444	1.5905	1.6276
	NP_score (top10%)	0.1482	0.1253	0.4336	0.8051	1.247	2.1975	2.3935	2.5946
	Structural Diversity		0.8356	0.8206	0.8231	0.8295	0.8347	0.7752	0.7529
NP score, SAS	NP_score	-1.3122	-1.0196	-0.7919	-0.5082	-0.2151	0.0759	0.9727	1.314
	NP_score (top10%)	0.1482	0.1253	0.3403	0.86	1.3508	1.7946	2.7121	2.9791
	SAS	3.0535	3.2642	2.8367	2.6373	2.621	2.2284	2.3073	2.7489
	SAS (top10%)	1.9545	2.0544	1.6902	1.525	1.5213	1.3358	1.2841	1.4864
	Structural Diversity		0.8356	0.8166	0.8122	0.8245	0.801	0.8042	0.8342
logP, DRD2	logP	2.4583	1.892	2.751	3.3405	3.7416	4.3834	8.3201	7.0397
	logP (top10%)	4.6321	4.2461	4.9568	5.5338	5.934	7.0267	10.7406	8.1715
	DRD2	0.0048	0.0066	0.0183	0.0374	0.0693	0.1477	0.5464	0.3587
	DRD2 (top10%)	0.0386	0.058	0.1572	0.3028	0.5151	0.8123	0.9971	0.9284
	Structural Diversity		0.8356	0.8203	0.8133	0.7989	0.7812	0.6088	0.5845
DRD2, SAS	DRD2	0.0048	0.0066	0.0085	0.021	0.0217	0.1063	0.424	0.5253
	DRD2 (top10%)	0.0386	0.058	0.0734	0.1937	0.1996	0.7922	1	0.9953
	SAS	3.0535	3.2642	2.7897	2.3898	2.2327	1.958	1.9466	2.1307
	SAS (top10%)	1.9545	2.0544	1.7315	1.4765	1.3778	1.2675	1.1678	1.2093
	Structural Diversity		0.8356	0.8148	0.7932	0.776	0.7311	0.6509	0.4659
NP score, DRD2	NP_score	-1.3122	-1.0196	-0.5209	-0.308	0.0339	0.7343	1.3774	1.8645
	NP_score (top10%)	0.1482	0.1253	0.5555	0.8434	1.3966	2.3955	2.4835	2.9185
	DRD2	0.0048	0.0066	0.0179	0.0384	0.0412	0.0859	0.2032	0.0744
	DRD2 (top10%)	0.0386	0.058	0.1454	0.3052	0.3116	0.6029	0.933	0.5707
	Structural Diversity		0.8356	0.8497	0.8518	0.8526	0.8531	0.8268	0.823

Table 2: Average property values of the training data and 1000 molecules randomly selected from the latent space of the initial model and the model learned after  $10^{th}$  iteration of weighted retraining for Task 1. For the top 10% average value, molecules are ranked according to the corresponding property.

A.2 Effect of weight parameter  $k$  in Task 2

Pair	Property	Training data	Initial Model	Model after $10^{th}$ retraining with					
				$k = 10^{-1}$	$k = 10^{-2}$	$k = 10^{-3}$	$k = 10^{-4}$	$k = 10^{-5}$	$k = 10^{-6}$
logP, SAS	logP	2.0875	1.6463	2.4422	2.7768	3.0227	3.2961	4.6374	5.7802
	logP (top10%)	3.8794	4.016	4.6657	4.8221	5.0974	5.4151	6.9437	8.3022
	SAS	3.2455	3.5983	3.1535	3.0309	2.8112	2.7935	2.077	1.5667
	SAS (top10%)	2.2257	2.2641	2.0878	1.9964	1.8365	1.8263	1.252	1.0853
	Structural Diversity		0.8474	0.8319	0.822	0.82	0.8098	0.7441	0.5793
logP, NP score	logP	2.2063	1.7481	2.305	2.4386	2.6125	2.8047	4.1676	7.7328
	logP (top10%)	4.0605	4.003	4.6038	4.7897	5.1549	5.3801	7.1442	10.6178
	NP_score	-1.4805	-1.1313	-0.9178	-0.8948	-0.8349	-0.6123	-0.5973	0.0025
	NP_score (top10%)	-0.4047	0.0479	0.1571	0.1556	0.2705	0.49	0.4912	1.1428
	Structural Diversity		0.8404	0.8332	0.8312	0.8302	0.8376	0.7917	0.697
NP score, SAS	NP_score	-1.4945	-1.1036	-0.9777	-0.918	-0.8978	-0.8154	-0.4006	0.5817
	NP_score (top10%)	-0.434	0.0183	0.1405	0.1754	0.2748	0.4079	1.2818	1.4811
	SAS	3.0918	3.4395	3.2631	3.164	3.0964	3.0436	2.3313	1.9048
	SAS (top10%)	2.1067	2.1432	2.0527	1.9997	1.9438	1.7133	1.294	1.1261
	Structural Diversity		0.8411	0.8364	0.8338	0.8323	0.8375	0.8144	0.7737
logP, DRD2	logP	2.2028	1.8422	2.2442	2.6281	2.8932	3.0949	3.7252	9.9092
	logP (top10%)	4.0734	4.1474	4.606	4.8051	5.196	5.3806	6.1771	21.8808
	DRD2	0.001	0.0028	0.0075	0.0159	0.0244	0.0216	0.0278	0.181
	DRD2 (top10%)	0.0053	0.0203	0.0607	0.1337	0.2061	0.1778	0.2206	0.8569
	Structural Diversity		0.8351	0.8333	0.8319	0.831	0.8288	0.7987	0.7148
DRD2, SAS	DRD2	0.0013	0.0044	0.0084	0.0084	0.0081	0.009	0.0356	0.1094
	DRD2 (top10%)	0.0071	0.0358	0.0732	0.072	0.07	0.0779	0.3287	0.7098
	SAS	3.1799	3.4301	3.313	3.1823	2.9907	2.9342	2.2998	1.6668
	SAS (top10%)	2.1636	2.1501	2.0841	2.0245	1.9232	1.8324	1.5063	1.1516
	Structural Diversity		0.8452	0.8364	0.8334	0.8325	0.8315	0.8012	0.7252
NP score, DRD2	NP_score	-1.5318	-1.2088	-0.9943	-0.8575	-0.7821	-0.6855	-0.4658	0.7919
	NP_score(top10%)	-0.5758	-0.1227	0.0749	0.2002	0.2949	0.414	0.8877	1.932
	DRD2	0.0008	0.0041	0.012	0.0116	0.0204	0.02	0.0562	0.2996
	DRD2 (top10%)	0.0041	0.035	0.1061	0.0966	0.1695	0.1692	0.4658	0.9653
	Structural Diversity		0.8279	0.8367	0.837	0.8377	0.8416	0.8313	0.7327

Table 3: Average property values of the training data and 1000 molecules randomly selected from the latent space of the initial model and the model learned after  $10^{th}$  iteration of weighted retraining for Task 2. For the top 10% average value, molecules are ranked according to the corresponding property.